Micromagnetic structure of domains in Co/Pt multilayers. I. Investigations of wall structure

Cite as: Journal of Applied Physics **74**, 7431 (1993); https://doi.org/10.1063/1.354964
Submitted: 11 May 1993 . Accepted: 05 August 1993 . Published Online: 17 August 1998

R. Ploessl, J. N. Chapman, M. R. Scheinfein, J. L. Blue, M. Mansuripur, and H. Hoffmann

Micromagnetic structure of domains in Co/Pt multilayers. I. Investigations of wall structure

R. Ploessl[a] and J. N. Chapman
Department of Physics and Astronomy, University of Glasgow, Glasgow G12 8QQ, United Kingdom

M. R. Scheinfein
Department of Physics and Astronomy, Arizona State University, Tempe, Arizona 85287-1504

J. L. Blue
Applied and Computational Mathematics Division, National Institute of Standards and Technology, Gaithersburg, Maryland 20899

M. Mansuripur
Optical Science Center, University of Arizona, Tucson, Arizona 85721

H. Hoffmann
Institut für Angewandte Physik, Universität Regensburg, 93040 Regensburg, Germany

(Received 11 May 1993; accepted for publication 5 August 1993)

An analysis of the micromagnetic structure of domains and domain walls in Co/Pt multilayer films is reported. Magneto-optically written domains have been imaged in a scanning transmission electron microscope by using the modified differential phase contrast mode of Lorentz electron microscopy. These have been compared with computer-simulated images based on a two-dimensional model of a circular, perpendicular magnetized domain with a Bloch-like wall structure. Agreement is found for the domain and stray field contrast, but the absence of wall contrast in the experimental images indicates a more complex wall structure in the multilayer than was assumed by the model. In a further series of calculations the magnetic microstructure of a Co/Pt multilayer was modeled by solving the Landau–Lifshitz–Gilbert equations. These suggest that the wall structure varies throughout the thickness of the multilayer, allowing significant saving of magnetostatic energy through the establishment of flux closure paths close to the walls, and are consistent with experimental observations.

I. INTRODUCTION

Co/Pt multilayer structures have been demonstrated to be a favorable candidate for a second-generation magneto-optical (MO) or thermomagnetic recording medium.[1–3] The main advantages offered by such multilayer materials include control of magnetic and MO properties through variation of the individual layer thicknesses, superior resistance to oxidation, and potentially higher storage densities at shorter wavelengths.

A detailed knowledge of the micromagnetic structure of MO domains is important for a better understanding of the magnetic properties of Co/Pt films in order to facilitate further improvements. The differential phase contrast (DPC) imaging mode of Lorentz transmission electron microscopy (TEM) provides a powerful means by which this information can be obtained. Differential phase contrast is a linear imaging mode and allows the spatial variation of the magnetic induction component perpendicular to the electron trajectory to be determined quantitatively. Both film magnetization and stray fields, which are always present in perpendicular media, are detected and contribute to the image contrast.

Our experimental investigations using the electron microscope are linked to two separate series of computer simulation studies: The first of these allows efficient and rapid computation of the image contrast of a magnetic thin film with a defined micromagnetic structure. Here we have chosen to model a circular domain in a perpendicular medium. This enables us to compare the observed with the simulated image contrast. The second series of computer programs calculates the micromagnetic structure of the domain-wall region in the multilayer by solving the Landau–Lifshitz–Gilbert equation. In these programs a relaxation scheme is used to determine the equilibrium magnetization configuration.

The rest of this article is structured as follows: Section II gives a brief outline of the DPC imaging mode and its modified implementation when studying micropolycrystalline materials. In Sec. III the experimental results on MO domains in Co/Pt films are discussed. Section IV shows how DPC contrast can be modeled and compares observed and predicted results. Section V describes the detailed wall structure found by micromagnetic simulation calculations of the multilayer stack and discusses its implications for the experimentally obtainable wall contrast in Co/Pt multilayer films.

II. EXPERIMENT

Various imaging modes of Lorentz electron microscopy have been used for the investigation of magnetic thin films and the domains they support.[4] The DPC mode,

[a]On leave from: Institut für Angewandte Physik, Universität Regensburg, 93040 Regensburg, Germany.

 0021-8979/93/74(12)/7431/7/$6.00

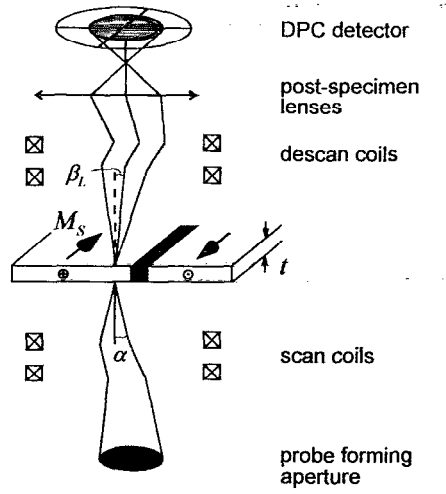

FIG. 1. Schematic of the DPC imaging mode (α: probe angle; t: film thickness; M_S: saturation magnetization; β_L: Lorentz angle).

which was used for all the experiments described below, has been explained in detail elsewhere[5–7] and is only outlined briefly here. It is implemented on a scanning transmission electron microscope (STEM) in which a focused electron probe is scanned across a magnetic sample (see Fig. 1). In a region of magnetic induction, the electron beam is deflected due to the Lorentz force toward a detector which is situated in the far field with respect to the specimen. The local deflection of the electron beam is measured by taking differences of the signals falling on opposite segments of a circular four-quadrant detector. The descan coils are used to ensure that in the absence of a specimen the difference signals are always zero.

The difference signals map the components of magnetic induction perpendicular to the electron trajectory and integrated along it. Thus films with perpendicular magnetization, such as MO media, have to be tilted in the microscope (see Fig. 2) in order to obtain a nonzero perpendicular magnetization component $M_\perp$. The orientation of the detector with respect to the specimen can be chosen freely by introducing rotation through variation of the excitations of the postspecimen lenses. In this article all DPC images map the components of induction along either the x or y axis of the image, with the black and white end of the grey scale denoting negative and positive vector components, respectively. As the difference signals from a quadrant detector register two orthogonal components of induction, it is straightforward to construct a vector map from a DPC image pair.[8]

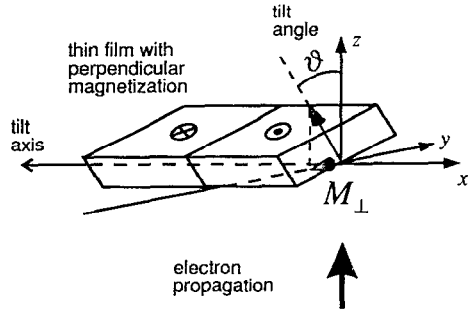

FIG. 2. Introduction of tilt to reveal magnetic contrast when imaging perpendicular magnetized specimens.

If small grain films are investigated, standard DPC images contain a considerable amount of crystalline contrast: The electrostatic potential changes rapidly at the grain boundaries and contributes to the phase gradients being detected. This problem can be alleviated by using a modified DPC detector which consists of the original solid quadrant detector extended by an annular quadrant detector.[6] If difference signals from only the outer detector are taken, the contrast transfer function of the imaging system changes. By careful selection of the size of the bright-field disk relative to the inner diameter of the detector, the experimenter can substantially enhance the relatively slowly varying magnetic contribution to the signal and suppress the unwanted contribution from the crystallites. Images acquired in this way are referred to as MDPC images. It has been demonstrated that MDPC imaging is capable of obtaining information about the micromagnetic structure of a polycrystalline magnetic thin film on the scale of ≈ 10 nm.[9] In our experiments digital MDPC images are acquired (with a resolution of 256×256 pixels and a precision of 8 bits/pixel) using a modified VG Instruments HB5 STEM.

III. EXPERIMENTAL RESULTS

The Co/Pt films investigated were prepared by e-beam evaporation[10] with a multilayer structure of 1.00 nm Pt $+15\times$(0.35 nm Co+1.08 nm Pt). The films were grown on top of a very thin Si_3Ni_4 membrane and as such were suitable for direct TEM investigation. No contrast from the thin amorphous membrane can be seen in the STEM images at the magnifications presented in this article. The coercivity of the film H_c determined from the Kerr hysteresis loop is 115 kA/m.

Figure 3 shows MDPC images of a thermomagnetically written domain. The domain was written at a bias field of 25 kA/m and a laser power of 10 mW. Four MDPC image pairs are displayed with two different tilt axes and positive and negative tilt angles. The elongated appearance of the circular domain is due to the specimen tilt. Because the films are perpendicularly magnetized the stronger contrast is always observed in the image which maps components perpendicular to the tilt axis, as would be expected from Fig. 2. Contrast reversal in these component images occurs when the tilt angle changes sign. In the other image, which maps induction components parallel to the tilt axis, the domain area itself shows negligible contrast change because of the absence of a magnetization component projected in this direction. No contrast whatsoever is seen from untilted samples.

The written domains are surrounded by a symmetric, alternating black and white pattern, which consists of four kidney-shaped areas with a rotation of 45° between the patterns in an image pair of a given domain. Again contrast

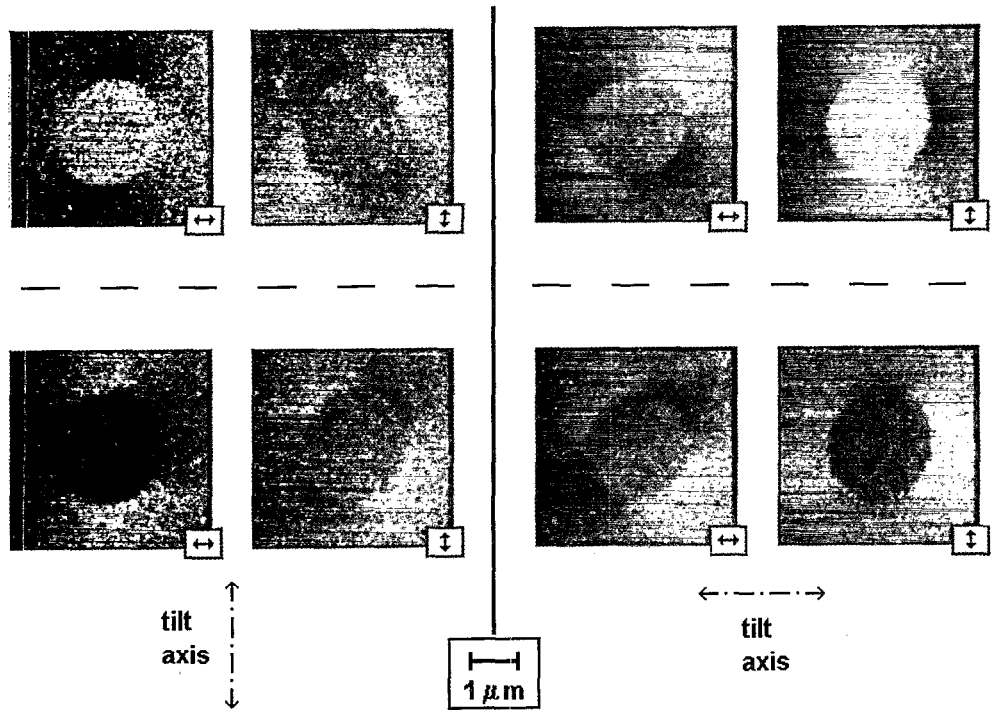

FIG. 3. Effects of specimen tilt on the observed MDPC contrast. The arrows denote the induction mapping direction.

reversal can be observed when the tilt angle is reversed, although the contrast here, arising from the stray fields which extend beyond the domain boundary, is somewhat smaller than the dominating domain contrast. Note that no stray field contrast would be expected from an untilted specimen because the fields above and below the specimen cancel out the deflection of the electron beam. The stray field can easily be visualized by constructing the vector induction map shown in Fig. 4 (calculated from the lower right image pair in Fig. 3). The vector pattern follows the flux closure path of the tilted cylindrical domain. We note that in this vector map the area which was used to calculate each vector is too large to display any detail of the domain boundary. However, higher-magnification images suggest that the transition region where the magnetization reverses direction is fairly abrupt, taking place over a distance <20 nm. Residual crystallite contrast and the size of the probe preclude a more precise estimate being made. A detailed discussion of the geometry that the domain boundary can assume is given in the companion article.

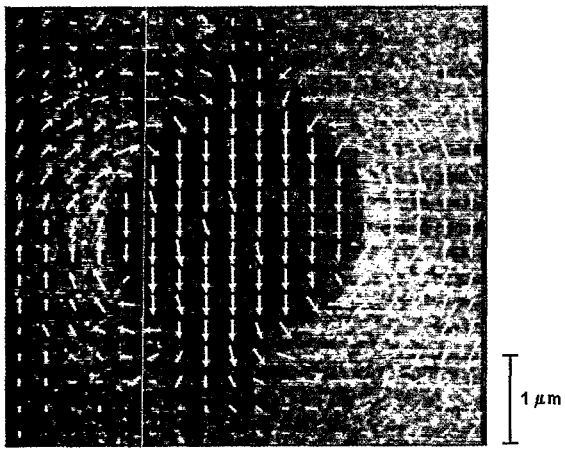

FIG. 4. Vector induction map of a written domain in Co/Pt showing the influence of the stray field on the observed contrast. The vector map is superimposed on the corresponding y component MDPC image.

IV. CONTRAST SIMULATION CALCULATIONS

The phase modulation that is imparted to the electron beam as it passes through a magnetic thin film can be calculated using a method introduced by Mansuripur.[11] The method calculates the phase function Φ resulting from a two-dimensional magnetization configuration by using fast Fourier transforms (FFTs).[12] The magnetization distribution is defined on a 256×256 grid which is assumed to be periodic along both x and y directions. The direction of magnetization at any point on the grid is modeled by the polar angle (measured from the z axis) and the azimuthal angle (measured from the x axis). Both angles are assumed not to vary along the z axis parallel to the film normal so that the system is truly two-dimensional. The specimen tilt can be chosen by varying the angle of incidence of the electron propagation vector on the film. The remaining input parameters necessary for the calculation are the grid lattice constant a_0, film thickness t, and saturation magnetization M_S.

In order to simulate a cylindrical domain in a perpendicular medium we used a Bloch-like wall structure described by an arctan or tanh function. The precise form of

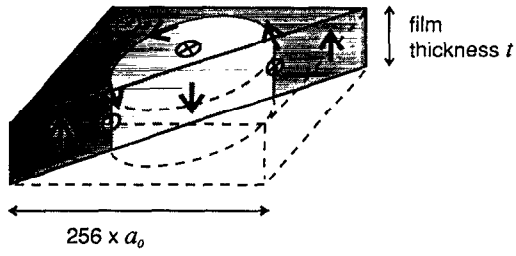

FIG. 5. Setup configuration of a circular, perpendicular magnetized domain for DPC contrast simulation calculations.

the analytical function for the wall profile has a negligible effect on the contrast. The setup configuration is drawn schematically in Fig. 5, the in-plane magnetization in the center of the wall following a flux closure path around the circumference of the domain; thus, there are no free magnetic poles on the wall surface. It is necessary to include an in-plane component in the wall configuration and a finite wall width δ_W, because a steplike wall profile is equivalent to an undersampling of the wall structure and leads to spurious aliasing effects introduced by the FFTs. In practice this places restrictions on the lattice grid constant which should satisfy the relation $a_0 \leqslant \delta_W/3$. We should further note that there is no reason *a priori* to expect that the magnetization should change direction discontinuously.

Once the phase function has been calculated it is straightforward to calculate its derivatives and hence the averaged induction components using the relations[5]

$$B_x = \nabla_y \Phi(x,y) C,$$

$$B_y = -\nabla_x \Phi(x,y) C,$$

where $C = \hbar/et$ ($\hbar$ is Planck's constant, e is the electron charge). The spatial variation of the derivatives can be regarded as idealized DPC images, namely, the images that would result if the only interaction between the electron beam and the specimen was magnetic in origin and the probe incident on the specimen was infinitesimally fine. In practice, of course, neither condition is fulfilled but by using MDPC imaging as described above and by realizing that the probe used in the experiments was ≈ 10 nm in diameter, it is to be expected that comparison of simulated and real DPC images will be meaningful.

Figure 6 shows a series of simulated image pairs displayed in the same order as the experimental MDPC images in Fig. 3. The parameters used are $M_S = 1400$ emu/cm^3, $t = 20$ nm, $a_0 = 5$ nm, and $\delta_W = 15$ nm. The M_S value is that appropriate to bulk cobalt while the thickness is simply the total cobalt thickness within the multilayer. It should be realized that the deflection angles are so small (typically < 2 μrad) that the separation of the layers has no effect on the deflection experienced by the beam. Furthermore, the form of the predicted contrast variation is very insensitive to the precise value chosen for M_S. Thus, negligible errors should arise from this source. The value for the wall width is more problematic in that very little work has been done on the nature of walls in perpendicular multilayer structures and we have assumed a value that is of the same order as we determined in previous work on pure cobalt films.[13] Bearing in mind the criterion previously discussed for the lattice grid constant we have an overall area of 1.28×1.28 μm^2 which allows us to simulate

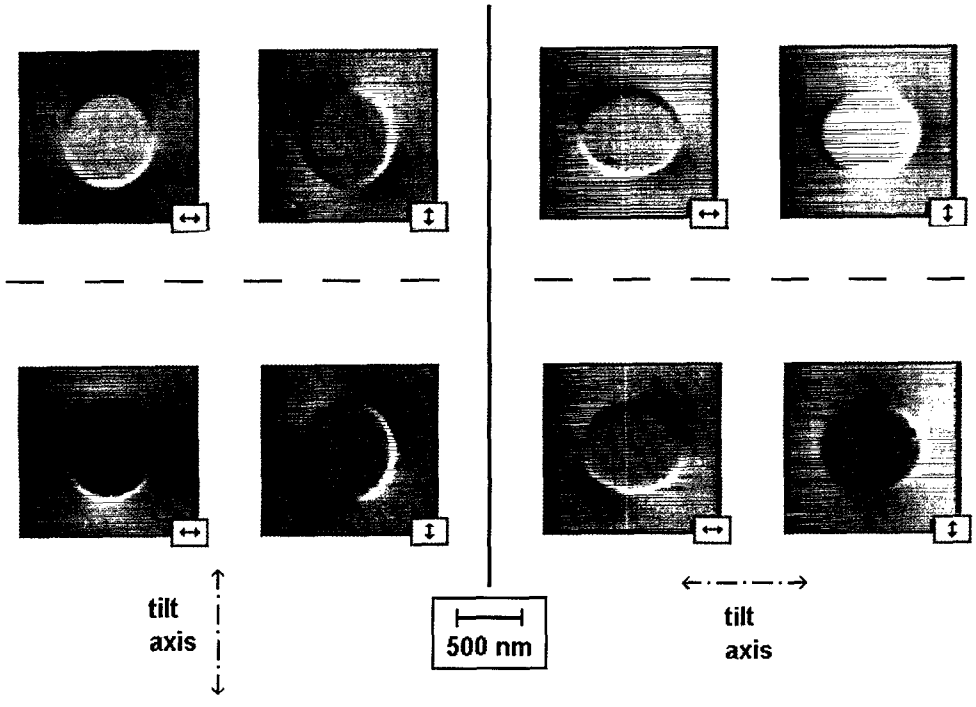

FIG. 6. Calculated DPC image contrast from the magnetization configuration of Fig. 5, shown for different tilt axes and angles and displayed as in Fig. 3.

images of domains $\approx$600 nm in diameter without suffering unduly from overlapping contrast from neighboring regions when the basic repeat area is periodically continued. Such domain sizes are only slightly smaller than those observed in practice.

Again the strongest contrast can be seen in the images which map induction components perpendicular to the tilt axis. The domain contrast agrees well with the experimental observations and also the stray field contrast is accurately predicted by the model. However, very strong wall contrast can be observed as narrow white and black bands at the circumference of the domain, following the flux closure path in the assumed wall configuration. This wall contrast is much stronger than the domain contrast (because the magnetization is in plane in the wall region) and this is in marked disagreement with experimental observation. Indeed wall contrast, of the form suggested by these model calculations, was never detected in any of the Co/Pt films we have investigated. A number of possibilities could explain the discrepancy. First, it is possible that the walls are sufficiently narrow that they effectively fall beyond the resolution limit of the technique. Extension of the model calculations to take account of the finite size of the probe suggest that this is unlikely and wall contrast would be visible albeit diminished. Furthermore, previous work[14] using very similar imaging conditions on large grain polycrystalline cobalt films has shown that wall contrast can be seen very easily even when the wall width and probe size are comparable. Thus a more likely explanation is that the actual wall structure in these multilayer films is more complex than a simple distribution that does not vary throughout the film thickness and that the use of essentially one-dimensional wall models is inappropriate. The micromagnetic calculations described in the following section support this conclusion.

V. MICROMAGNETIC WALL STRUCTURE CALCULATIONS

In order to gain more information on the wall structure in a Co/Pt film, the micromagnetic structure of the multilayer stack was modeled by solving the Landau–Lifshitz–Gilbert (LLG) equation[15] in a two-dimensional approximation. In the calculation we used a coordinate system ξ,η,z where, as in the previous sections of this article, z was perpendicular to the film surface. The computation was two-dimensional in the sense that the film was assumed to be infinite in the η direction so that $\mathbf{M}=\mathbf{M}(\xi,z)$. A discretized grid with about 6000 quadratic elements was used to model alternating ferromagnetic and nonferromagnetic layers. The size of these elements was 0.35 nm, so that the mesh was fine enough to reflect the dimension of a single Co layer. Precise parameters used in the model are shown in Table I and can be seen to closely resemble those of the multilayer under investigation experimentally. Differences do exist, however, in that the structure was terminated by a Co layer to obtain a symmetric structure, thus simplifying the treatment of the boundaries. Furthermore, it should be recognized from the outset that there are considerable dangers in using bulk parameters to calculate the magnetization distribution in a film whose individual layers are only one or two atom layers thick.

TABLE I. Parameters used in LLG micromagnetic domain wall simulations. Bulk parameters were selected for the Co layers. There was no exchange between neighboring Co and Pt layers and the Pt was assumed to be nonmagnetic.

Number of bilayers	n	15
Co layer thickness	t_{Co}	0.35 nm
Pt layer thickness	t_{Pt}	1.05 nm
Saturation magnetization	M_S	1400 emu/cm^3
Exchange parameter	A	0.31×10^{-5} erg/cm
Anisotropy	K_u	1.2–9.6×10^{6} erg/cm^3

The boundary conditions were set for the magnetization on the right- and left-hand side of the grid to point in the $+z$ direction, and at the beginning of the calculation the inner region of the grid was assumed to be above the Curie temperature. On "cooling," the magnetization was allowed to relax and an inversely magnetized domain formed in the center region of the mesh. An iterative relaxation procedure then allowed each magnetization vector to rotate in turn to lie along the local effective field vector as predicted from the LLG equations. The equilibrium micromagnetic structure results from the local minimization of the total energy through the balance of exchange, anisotropy, and magnetostatic energies. Details of these and the relaxation algorithm are found in Refs. 15 and 16. Although the relaxation method, unlike the time integration method of the LLG equation, does not guarantee a global energy minimum, it has been shown that both methods yield equivalent results in the calculation of 180° domain walls.[16]

Figure 7 shows the result for the multilayer structure under consideration. The vector map is based on a 108×10 mesh with only every fourth vector in each row being shown; the correct aspect ratio is maintained as each vector is plotted with its tail at its true position. All vectors are found to have ξ and z components only and no η components. The overall configuration shows a strong magnetization circulation around each wall leading to substantial

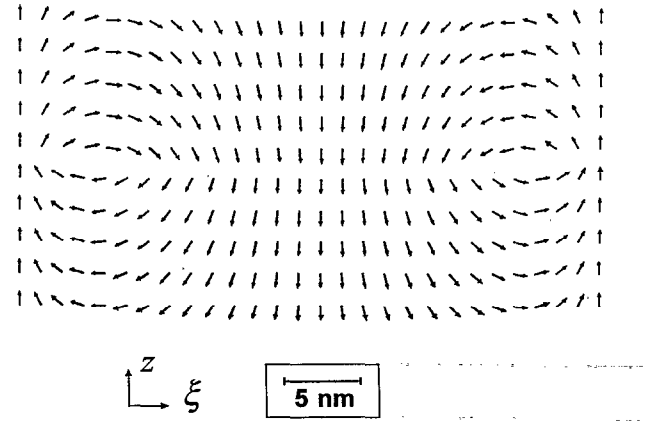

FIG. 7. Calculated magnetization pattern of the Co/Pt multilayer cross section.

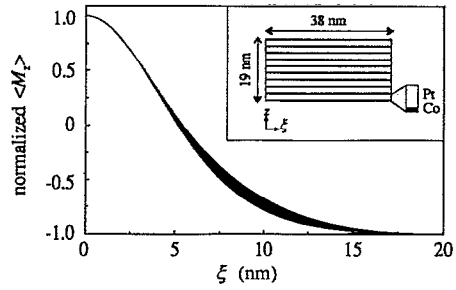

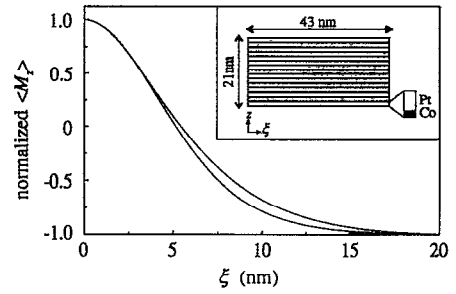

FIG. 8. Thickness-averaged wall profiles for different film geometries and anisotropies; steeper profiles correspond to higher anisotropy values; the insets show the correct proportions of the modeled multilayer structures: (a) wall profiles for 0.35 nm Co+15×(1.05 nm Pt+0.35 nm Co) and K_u=1.2, 2.4, 3.6, 4.8, 6.0, 7.2, 8.4, and 9.6×10^6 erg/cm^3; (b) wall profiles for 0.35 nm Co+9×(1.75 nm Pt+0.35 nm Co) and K_u=2.0 and 10.0×10^6 erg/cm^3.

flux closure. Wall widths reach a maximum at the film surfaces and are narrowest in the center planes of the multilayer.

This global magnetization pattern is found to be remarkably robust against changes in the Pt layer thickness or the number of bilayers in the stack. Thus, its essential features remain intact even when the number of Co layers is reduced to two. Minor changes only are recorded when the width of the grid is changed and modest variation of the bulk magnetization constants do not affect the pattern and only slightly alter the wall widths. To illustrate these points Fig. 8 shows how the averaged z components of magnetization vary for two different stack geometries and for a range of assumed anisotropy constants. As the latter increase, the wall width decreases slightly, the mean value being $\approx$10 nm. The wall profiles themselves display some asymmetry and this may reflect the boundary conditions enforced at the extremes of the grid.

The wall structures calculated in this section can be represented schematically as shown in Fig. 9 for circular domains. Unlike the structure shown in Fig. 5 there is no component of magnetization parallel to the wall. If an electron beam is transmitted through the new structure, the deflections due to the in-plane magnetization components in the wall cancel out and there is no deviation from the original path. Domain and stray field contrast, however, remain unchanged. This then leads to an overall contrast *distribution* which agrees with the experimental observations. We therefore believe that the micromagnetic structure as drawn in Fig. 9 is a more accurate model than the simple one-dimensional form presented in Sec. IV.

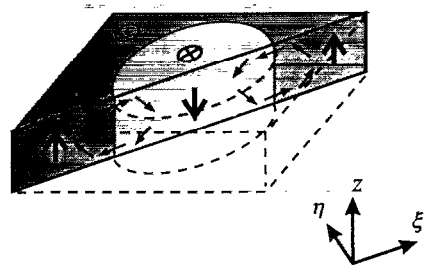

FIG. 9. Schematic of the micromagnetic structure of a circular, perpendicular magnetized domain with the wall structure of Fig. 7.

VI. DISCUSSION AND CONCLUSIONS

We have shown that modified DPC imaging is well suited to providing a good description of the micromagnetic structure of domains in MO multilayer materials. The MDPC image contrast of thermomagnetically written domains which was presented in Sec. III accurately reveals the domain geometry and the presence of stray fields beyond the specimen; these are in good agreement with the contrast simulations presented in Sec. IV. However, contrary to the predictions of simple models and to what is found in single-layer films, no wall contrast of any kind is observed experimentally. By solving the micromagnetic equations adapted for a multilayer structure we obtain the wall pattern introduced in Sec. V and, while there must be doubts about using such a model on a near atomic scale, its predictions are remarkably robust to parameter variation. Furthermore, the wall structure predicted is perfectly consistent with the experimental observations in terms of both scale and contrast.

The predicted wall structure seems very plausible and illustrates well the kind of difference that can arise in a multilayer film. Such a wall would never occur in a very thin continuous film because the exchange penalty involved in abruptly changing the sense of rotation of the in-plane component at the center of the film would be too high. Of course, in thicker films it is not unusual to find that at the surfaces the wall shows Néel-like behavior with opposite polarities observed at top and bottom. However, in these cases there is always an intervening Bloch-like section through the center of the film leading to the well-known vortex walls.[15,17] Here, the absence of exchange coupling between layers leads to no such restraints and offers the very attractive possibility of introducing a region where the magnetization forms a circulation path at the position of the wall. This represents a saving in magnetostatic energy which simply is not present in the Bloch wall geometry. Thus, as the anisotropy energy is likely to be similar whether we have Bloch- or Néel-like behavior it is not surprising that the micromagnetic calculation, which imposes no conditions about the sense in which the magneti-

zation should rotate, finds a lower energy state than would be possible with a simple one-dimensional variation.

ACKNOWLEDGMENTS

We would like to thank Dr. H. W. van Kesteren for provision of the multilayer samples. We gratefully acknowledge support from the CAMST (Community Action on Magnetic Storage Technology) scheme of the European Commission and the Science and Engineering Research Council of the U.K. R.P. acknowledges support from the European Commission under Contract No. BREU 900 320.

[1] F. J. A. M. Greidanus, W. B. Zeper, B. A. J. Jacobs, J. H. M. Spruit, and P. F. Carcia, Jpn. J. Appl. Phys. **28**, Suppl. 28-3, 37 (1989).
[2] W. B. Zeper, H. W. van Kesteren, B. A. J. Jacobs, and J. H. M. Spruit, J. Appl. Phys. **70**, 2264 (1991).
[3] W. B. Zeper, A. P. J. Jongenelis, B. A. J. Jacobs, H. W. van Kesteren, and P. F. Carcia, IEEE Trans. Magn. **MAG-28**, 2503 (1992).
[4] J. N. Chapman, J. Phys. D. **17**, 623 (1984).
[5] J. N. Chapman and G. R. Morrison, J. Magn. Magn. Mater. **35**, 254 (1983).
[6] J. N. Chapman, I. R. McFadyen, and S. McVitie, IEEE Trans. Magn. **MAG-26**, 1506 (1990).
[7] J. N. Chapman, R. Ploessl, and D. M. Donnet, Ultramicroscopy **47**, 331 (1992).
[8] I. R. McFadyen, J. Appl. Phys. **64**, 6011 (1988).
[9] R. Ploessl, J. N. Chapman, A. M. Thompson, J. Zweck, and H. Hoffmann, J. Appl. Phys. **73**, 2447 (1993).
[10] W. B. Zeper, F. J. A. M. Greidanus, P. F. Carcia, and C. R. Fincher, J. Appl. Phys. **65**, 4971 (1989).
[11] M. Mansuripur, J. Appl. Phys. **69**, 2455 (1991).
[12] M. Mansuripur and R. Giles, IEEE Trans. Magn. **MAG-24**, 2326 (1988).
[13] M. Labrune, J. Miltat, J. P. Jakubovics, A. M. Thompson, and J. N. Chapman, J. Magn. Magn. Mater. **104–107**, 343 (1992).
[14] J. N. Chapman, J. P. Jakubovics, and I. R. McFadyen, J. Magn. Magn. Mater. **54–57**, 847 (1986).
[15] A. E. LaBonte, J. Appl. Phys. **40**, 2450 (1969).
[16] M. R. Scheinfein and J. L. Blue, J. Appl. Phys. **69**, 7740 (1991).
[17] A. Hubert, Phys. Status Solidi **32**, 519 (1969).